ChemComm

COMMUNICATION

Check for updates

Cite this: *Chem. Commun.*, 2019, 55, 12008

Received 11th August 2019,
Accepted 9th September 2019

DOI: 10.1039/c9cc06211d

rsc.li/chemcomm

A selective colorimetric strategy for probing dopamine and levodopa through the mussel-inspired enhancement of Fe_3O_4 catalysis†

Mengyuan Yin,[a] Shuai Li,[a] Yuqi Wan,[a] Luping Feng,[b] Xiaoting Zhao,[a] Sheng Zhang,[a] Shuhui Liu,[a] Peng Cao[a] and Hua Wang *[ab]

Mussel-inspired enhancement of Fe_3O_4 catalysis was discovered towards a highly selective and sensitive colorimetric strategy for the magnetic separation-based evaluation of dopamine and/or levodopa in urine, in which the specific interaction of bis-catechol-containing analytes and mesoporous Fe_3O_4 NPs would form highly stable complexes of bis-catechol-Fe coordination.

Dopamine (DA) as a catecholamine neurotransmitter plays a vital role in the human central nervous system, thus serving as a biomarker with indicative levels (normally at μM levels in urine) for some serious diseases like schizophrenia and Parkinson's diseases.[1–4] For example, Parkinson's disease as a progressive neurodegenerative disorder occurs due to the DA deficiency in the brain, for which the clinical treatment drug levodopa (LDA) has generally been applied to metabolically yield DA for compensating the DA deficiency.[5,6] Therefore, it is of great medical significance to monitor the levels of DA and/or LDA in human metabolites like urine for the accurate diagnosis and therapeutic drug monitoring of these diseases.[7,8] To date, many classical detection methods have been developed for sensing DA or LDA, such as high-performance liquid chromatography,[9] fluorimetric analysis,[10] capillary electrophoresis,[11] chemiluminescence,[12] and chromatography methods.[13] Most of them, however, may encounter some intrinsic disadvantages like expensive facilities, tedious operation, and complicated sample pre-treatment. In recent decades, the development of electroanalysis methods as the preferable detection candidates with portable devices for on-site applications for probing DA has aroused a lot interest.[14–17] Nevertheless, they may be generally interfered with by some electroactive small molecules like ascorbic acid (AA) and uric acid (UA) with electrochemical outputs at very close potentials showing low selectivity for the analysis of DA especially those in complex biological samples. Moreover, colorimetric detection technologies have been applied alternatively for the detection of DA.[4,18–22] For example, Booth *et al.* have designed an etching-based colorimetric method for sensing DA using pyridinium-decorated silver nanoparticles.[21] Wilson and colleagues fabricated a microfluidic paper-based analytical device for the colorimetric DA assay.[22] However, the current colorimetric methods may usually be hindered either by low analysis selectivity or poor detection sensitivity.

Recent years have witnessed the rapid development of catalytic nanomaterials, known as nanozymes, such as ultra-small noble metals (*i.e.*, Pt, Au, and Ag) and Fe_3O_4 nanoparticles (NPs).[23–26] As nanozyme representatives, Fe_3O_4 NPs have been well recognized to intrinsically possess peroxidase-like catalysis together with the advantages of magnetic separation for wide biosensing applications.[26–30] However, the catalytic performances of Fe_3O_4 NPs may mainly depend on the particle sizes,[26] of which the larger ones can commonly present lower catalytic activities but higher magnetic properties. As a result, many arduous efforts have been devoted to the enhancement of the catalytic activities of Fe_3O_4 NPs for the extensive catalysis applications.[30–33] For example, Liu *et al.* applied phosphate backbone-containing DNAs to coat Fe_3O_4 NPs achieving accelerated catalysis.[30] Chen and co-authors doped Cu elements into Fe_3O_4 NPs resulting in enhanced catalysis for organic wastewater treatment.[31] Besides, DA as a mussel secreta with bis-catechol groups can undergo a powerful interaction with Fe ions to form Fe–dopa bonds so as to ensure that mussels firmly adhere onto the Fe-containing rocks, of which the interaction force can be so strong that its breaking requires a force similar to the one required for rupturing a covalent bond.[34] The resulting bis-catechol-Fe coordination complexes can enjoy extremely high known stability constants ($\log K_S \approx 37$–40).[35–37] Therefore, DA has been widely employed to mediate the mussel-inspired adsorption or immobilization of some biological molecules or functional probes onto magnetic Fe_3O_4 NPs like DNAs,

[a] *Institute of Medicine and Materials Applied Technologies, College of Chemistry and Chemical Engineering, Qufu Normal University, Qufu City, Shandong Province 273165, P. R. China. E-mail: huawang@qfnu.edu.cn; Web: http://wang.qfnu.edu.cn; Fax: +86 5374456306; Tel: +86 5374456306*

[b] *School of Chemistry and Chemical Engineering, Harbin Institute of Technology, Harbin, Heilongjiang 150090, P. R. China*

† Electronic supplementary information (ESI) available. See DOI: 10.1039/c9cc06211d

This journal is © The Royal Society of Chemistry 2019

enzymes, and antibodies.[38–41] For example, a fluorescent biosensor has been developed for the detection of DNAs by using DA-coated Fe_3O_4 NPs to adsorb the products of hybridization chain reactions.[40] Also, enzymes were directly immobilized onto the DA-modified Fe_3O_4 NPs to fabricate amperometric biosensors for detecting phenolic compounds.[41] Besides, our group utilized DA to coat nano-scaled TiO_2 onto Fe_3O_4 NPs for photocatalytic silver deposition for the sensitive analysis of microRNAs.[38] Unfortunately, the fact that DA can enhance the intrinsic catalytic activity of Fe_3O_4 NPs has been generally ignored to date.

In the present work, mesoporous Fe_3O_4 NPs were originally fabricated by using an ethanediol-based solvothermal synthesis route (Scheme 1A). It was discovered that in addition to strong magnetism, the as-fabricated Fe_3O_4 NPs could present intrinsically a little catalysis in the chromogenic reactions of 3,3,5,5-tetramethylbenzidine (TMB) and hydrogen peroxide (H_2O_2). Unexpectedly, dramatically enhanced peroxidase-like catalytic activities of Fe_3O_4 NPs could be achieved once coated with DA or its derivatives like LDA (Scheme 1B). More importantly, the catalytic activities of Fe_3O_4 NPs can rationally depend on the amounts of DA or LDA, whereas other kinds of small molecules (*i.e.*, AA and UA) could display no significant interference. Herein, DA and LDA containing bis-catechol groups can undergo strong interaction with Fe_3O_4 NPs through specific chelation with the Fe ions of Fe_3O_4 NPs by forming highly stable complexes of bis-catechol-Fe coordination complexes (Scheme 1C), with extremely high known stability constants.[35,36] Furthermore, the DA so coated might be oxidized to produce quinone species (known as potent electron acceptors) to boost the electron transferring process of nanozymes of Fe_3O_4 NPs towards increased catalytic performances. A highly selective colorimetric strategy with magnetic Fe_3O_4 NPs was thereby developed for the magnetic separation-based evaluation of DA and LDA in urine. To the best of our knowledge, this is the first discovery of the DA or LDA-triggered enhancement of catalysis of Fe_3O_4 NPs for the colorimetric assays for DA and/or LDA.

The morphological structure of the as-prepared Fe_3O_4 NPs was characterized by using scanning electronic microscopy (SEM) (Fig. 1A). It is noted that Fe_3O_4 NPs could display a uniform spherical structure with an average size of about 485 nm in diameter. In particular, they could display a mesoporous structure as clearly revealed by the high-resolution transmission electron microscopy (TEM) image (Fig. 1A, inset), which may provide a large specific surface area available for DA or LDA coatings in addition to the strong magnetism. Furthermore, the catalytic performances of Fe_3O_4 NPs coated with DA or LDA were investigated based on the catalytic TMB–H_2O_2 reactions, taking the native Fe_3O_4 NPs, DA, and LDA as the controls (Fig. 1B). The results indicate that Fe_3O_4 NPs could display a greatly enhanced catalytic activity once coated with DA or LDA, which is more than four-fold higher than that of native Fe_3O_4 NPs, as visually witnessed in the photographs of the reaction solutions (inset). Moreover, catalytic dynamic studies were colorimetrically carried out for Fe_3O_4 NPs in the presence of DA as a model in comparison with native Fe_3O_4 NPs, with the data shown in Fig. S1 (ESI†). As described in Fig. S1A (ESI†), Fe_3O_4 NPs with DA could exhibit much better catalytic performances than native Fe_3O_4 NPs in terms of the catalytic reaction rates and response range of H_2O_2 concentrations, which was also observed for the TMB substrate (Fig. S1B, ESI†). An outstanding ability for tolerating toxic H_2O_2 could also be expected for Fe_3O_4 NPs in the presence of DA, which could exhibit no significant change in catalysis in H_2O_2 up to 200 mM (Fig. S1A, ESI†). Furthermore, double reciprocal plotting was performed to explore the catalytic activities of Fe_3O_4 NPs with and without DA separately for the substrates of H_2O_2 and TMB (Fig. S1C and D, ESI†). According to Lineweaver–Burk plots and the Michaelis–Menten equation, kinetic parameters like the apparent Michaelis

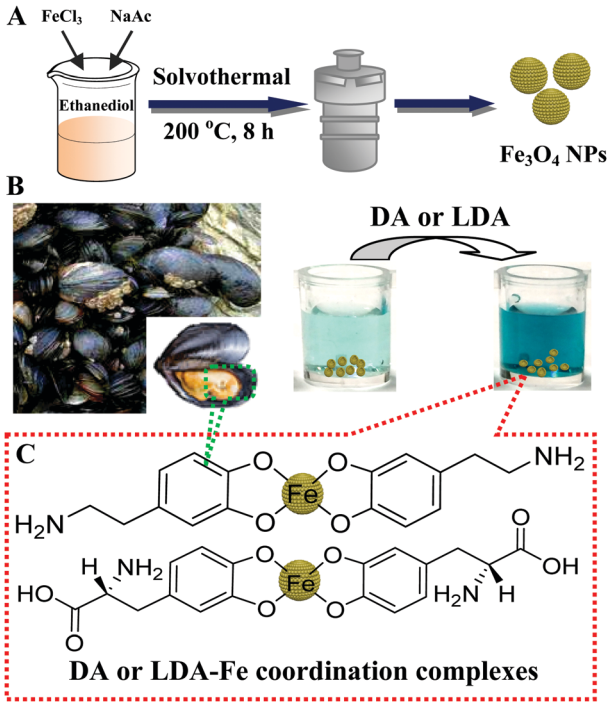

Scheme 1 (A) The synthesis procedure for mesoporous Fe_3O_4 NPs by a solvothermal route; (B) the mussel-inspired enhancement of Fe_3O_4 NP catalysis upon adding DA or LDA; (C) the molecular structures of DA and LDA and their bis-catechol-Fe coordination complexes formed on Fe_3O_4 NPs.

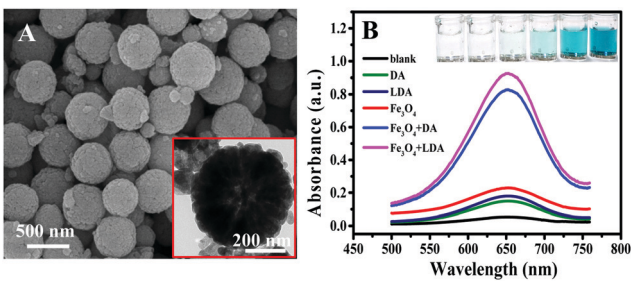

Fig. 1 (A) SEM images of Fe_3O_4 NPs (inset: a TEM image of Fe_3O_4 NPs with a magnitude-amplified view); (B) comparable investigations on the peroxidase-like catalytic activities of Fe_3O_4 NPs with DA or LDA, taking native Fe_3O_4 NPs, DA, and LDA as the controls (inset: the photographs of the corresponding reaction solutions).

constant (K_m) were calculated, with the results comparably summarized in Table S1 (ESI†). It is found that Fe_3O_4 NPs with DA can exhibit a lower K_m for TMB (0.2445 mM) than the native Fe_3O_4 NPs (0.3923 mM), indicating a higher affinity for the TMB substrate. Yet, they can present a higher K_m for the H_2O_2 substrate (54.04 mM) than the native Fe_3O_4 NPs (18.48 mM). These data indicate that the introduction of DA can endow Fe_3O_4 NPs with the improved catalytic activities, indicating that it should be feasible for the catalysis-based colorimetric analysis of DA and/or LDA.

Catalysis-selective colorimetric analysis of DA and LDA was carried out by comparing with other kinds of small molecules, amino acids, and ions (Fig. 2). One can note from Fig. 2A that the tested small molecules and amino acids could present negligible responses in comparison with that of DA or LDA, as well as the common ions indicated in Fig. 2B. Notably, the interference of other small molecules with a similar molecular structure, *i.e.*, tyramine and tyrosine with mono-catechol groups, could also display no influence on the colorimetric responses to DA and LDA, showing high analysis specificity. As aforementioned, this high detection selectivity of the Fe_3O_4 NP catalysis-based colorimetric method for DA or LDA containing bis-catechol groups should be due to the formation of much more stable bis-catechol-Fe complexes, which have known stability constants much higher than those of other kinds of analytes including the ones with mono-catechol groups mentioned above. Besides, DA or LDA coated on Fe_3O_4 NPs might be oxidized to produce active quinone species for accelerating the electron transferring process towards the enhanced catalysis of Fe_3O_4 NPs, ensuring the highly selective analysis of DA and/or LDA.

Colorimetric studies were further conducted comparably on the catalytic activities of Fe_3O_4 NPs in the presence (curve a) and absence (curve b) of DA under different catalytic reaction conditions, mainly including the dosages of Fe_3O_4 NPs, temperature, pH values, and ionic strengths in NaCl concentrations (Fig. S2, ESI†). It was found that both of the Fe_3O_4 NPs with and without DA could basically share similar optimal conditions of catalytic TMB–H_2O_2 reactions, including 0.0050 mg mL^{-1} Fe_3O_4 NPs (Fig. S2A, ESI†), 37 °C (Fig. S2B, ESI†), and acidic conditions like pH 3.0 (Fig. S2C, ESI†), which should be considered as the optimized conditions for the detection of DA and LDA. Also, the ionic strengths might have no significant effect on the catalytic reactions of DA or LDA-coated Fe_3O_4 NPs, and even the media might contain high salts with NaCl concentrations up to 300 mM (Fig. S2D, ESI†). Moreover, Fe_3O_4 NPs with DA could display much faster catalysis than the native Fe_3O_4 NPs, as revealed in Fig. S3A (ESI†). Besides, Fig. S3B (ESI†) shows that the high storage stability of Fe_3O_4 NPs, which could show no significant change in catalysis, was maintained even up to six months at room temperature. These experimental results indicate that in addition to high environmental stability, mesoporous Fe_3O_4 NPs could exhibit greatly enhanced catalytic performances in the presence of DA or LDA under the optimized conditions.

Under the optimized conditions, the developed Fe_3O_4 NP catalysis-based colorimetric detection method was employed to probe DA and/or LDA with different concentrations (Fig. 3). Fig. 3A shows the calibration curve of the catalysis-selective colorimetric detection for different concentrations of DA in buffer, of which the absorbance values could rationally increase with the increasing DA concentrations (inset). Accordingly, DA can be detected in concentrations linearly ranging from 0.010 to 4.0 μM, with a limit of detection (LOD) of about 3.5 nM, as estimated by the 3σ rule. Meanwhile, one can see from Fig. 3B that LDA can be determined in linear concentrations ranging from 0.0035 to 7.0 μM, with an LOD of about 2.5 nM. Moreover, Fig. 3C describes the detection curve of the colorimetric analysis for DA with different concentrations spiked in urine, showing the detection range from 0.025 to 9.7 μM, and an LOD of about 8.0 nM. Also, LDA in urine can be evaluated with the levels linearly ranging from 0.020 to 10 μM, with an LOD of about 5.0 nM (Fig. 3D). These quantitative responses to DA or LDA in samples can also be visualized from the photographs of the typical reaction solutions tested (Fig. 3, inset). In addition, a high detection reproducibility could be expected

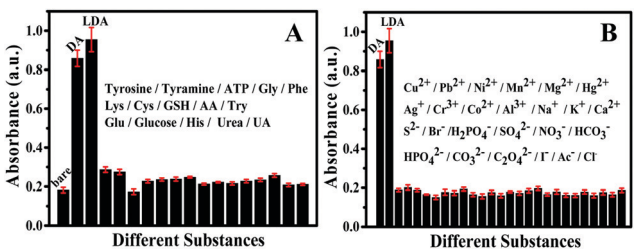

Fig. 2 Catalysis-based colorimetric responses of Fe_3O_4 NPs (0.0050 mg mL^{-1}) separately to (A) various small molecules and (B) different ions indicated (1.0×10^{-5} M).

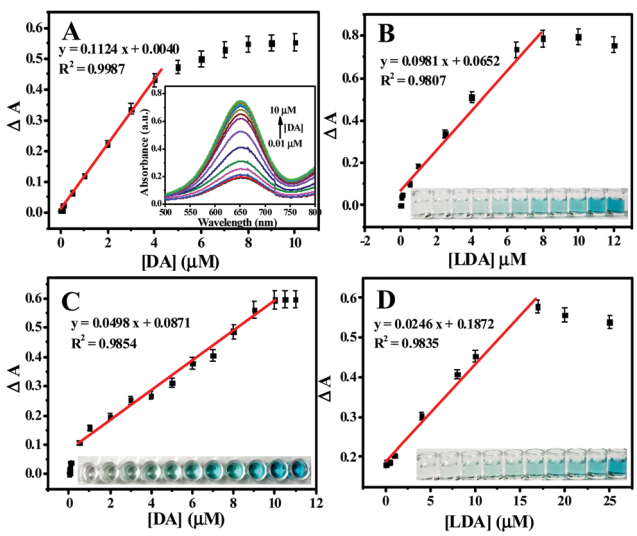

Fig. 3 The calibration curves of the Fe_3O_4 NP catalysis-based colorimetric method for the detection of (A) DA (inset: the corresponding absorption spectra of catalytic TMB–H_2O_2 reactions) and (B) LDA with different concentrations in buffer (inset: the photographs of the corresponding product solutions). The relationships between the absorbance changes *versus* (C) DA or (D) LDA concentrations in urine.

This journal is © The Royal Society of Chemistry 2019

for the developed colorimetric method, showing no significant change in the DA responses for the five repeated tests (data not shown). It is worth pointing out that the colorimetric analysis of the overall DA and LDA in urine should be expected. Therefore, the developed Fe_3O_4 NP catalysis-based colorimetric strategy can have promising practical applications for probing DA and/or LDA in human metabolites like urine with high analysis selectivity and sensitivity.

In summary, Fe_3O_4 NPs were fabricated with a mesoporous structure with a large specific surface area. In particular, the mussel-inspired enhancement of the peroxidase-like catalysis of Fe_3O_4 NPs was discovered towards a catalysis-selective colorimetric strategy for evaluating DA and its derivative LDA in urine. The detection mechanism is thought to rely on that DA or LDA with bis-catechol groups can specifically undergo strong interaction with the Fe ions of Fe_3O_4 NPs by forming stable bis-catechol-Fe coordination complexes with extremely high known stability constants. Meanwhile, the bis-catechol-containing compounds coated on Fe_3O_4 NPs might be oxidized to produce active quinone species so as to boost the electron transferring process towards the increased catalysis of nanozymes. The developed colorimetric method can enable the fast evaluation of DA and LDA in urine, with levels down to 8.0 nM and 5.0 nM, respectively, thus indicating promising clinical applications for the diagnosis and drug monitoring of DA-indicative diseases, respectively.

This work was supported by the National Natural Science Foundation of China (No. 21675099) and the Major Basic Research Program of Natural Science Foundation of Shandong Province (ZR2018ZC0129), Shandong, P. R. China.

Conflicts of interest

There are no conflicts to declare.

Notes and references

1 T. V. Maia and M. J. Frank, *Biol. Psychiatry*, 2017, **81**, 52–66.
2 F. A. Zucca, J. Segura-Aguilar, E. Ferrari, P. Munoz, I. Paris, D. Sulzer, T. Sarna, L. Casella and L. Zecca, *Prog. Neurobiol.*, 2017, **155**, 96–119.
3 Q. Wang, X. Zhang, L. Huang, Z. Zhang and S. Dong, *ACS Appl. Mater. Interfaces*, 2017, **9**, 7465–7471.
4 C. M. Perkinsbr, *J. Obstet. Gynaecol.*, 1982, **89**, 123–127.
5 R. A. Hawkins, A. Mokashi and I. A. Simpson, *Exp. Neurol.*, 2005, **195**, 267–271.
6 E. R. Ritvo, A. Yuwiler, E. Geller, A. Kales, S. Rashkis, A. Schicor, S. Plotkin, R. Axelrod and C. Howard, *J. Autism Child. Schizophr.*, 1971, **1–2**, 190–205.
7 Z. Wang, H. Y. Yue, Z. M. Yu, S. Huang, X. Gao, B. Wang, S. S. Song, E. H. Guan, W. Q. Wang and H. J. Zhang, *Microchem. J.*, 2019, **147**, 163–169.
8 G. Hu, L. Chen, Y. Guo, X. Wang and S. Shao, *Electrochim. Acta*, 2010, **55**, 4711–4716.
9 N. Li, J. Guo, B. Liu, Y. Yu, H. Cui, L. Mao and Y. Lin, *Anal. Chim. Acta*, 2009, **645**, 48–55.
10 D. Seto, T. Maki, N. Soh, K. Nakano, R. Ishimatsu and T. Imato, *Talanta*, 2012, **94**, 36–43.
11 Y. Zhao, S. Zhao, J. Huang and F. Ye, *Talanta*, 2011, **85**, 2650–2654.
12 M. Saqib, S. Bashir, H. Li, S. Wang and Y. Jin, *Anal. Chem.*, 2019, **91**, 3070–3077.
13 F. D. Ferreira, L. I. Silva, A. C. Freitas, T. A. Rocha-Santos and A. C. Duarte, *J. Chromatogr. A*, 2009, **1216**, 7049–7054.
14 E. E. Ferapontova, *Electrochim. Acta*, 2017, **245**, 664–671.
15 C. Yang, K. Hu, D. Wang, Y. Zubi, S. T. Lee, P. Puthongkham, M. V. Mirkin and B. J. Venton, *Anal. Chem.*, 2019, **91**, 4618–4624.
16 Q. He, J. Liu, X. Liu, G. Li, D. Chen, P. Deng and J. Liang, *Electrochim. Acta*, 2019, **296**, 683–692.
17 Q. He, J. Liu, X. Liu, G. Li, P. Deng and J. Liang, *Sensors*, 2018, **18**, 199–211.
18 J. Lian, P. Liu, X. Li, B. Bian, X. Zhang, Z. Liu, X. Zhang, G. Fan, L. Gao and Q. Liu, *Colloids Surf., A*, 2019, **565**, 1–7.
19 M. X. Guo and Y. F. Li, *Spectrochim. Acta, Part A*, 2019, **207**, 236–241.
20 Y. Wang, L. Yang, Y. Liu, Q. Zhao, F. Ding, P. Zou, H. Rao and X. Wang, *Microchim. Acta*, 2018, **185**, 496–504.
21 S. Rostami, A. Mehdinia, A. Jabbari, E. Kowsari, R. Niroum and T. J. Booth, *Sens. Actuators, B*, 2018, **271**, 64–72.
22 C. Liu, F. A. Gomez, Y. Miao, P. Cui and W. Lee, *Talanta*, 2019, **194**, 171–176.
23 Z. Sun, N. Zhang, Y. Si, S. Li, J. Wen, X. Zhu and H. Wang, *Chem. Commun.*, 2014, **50**, 9196–9199.
24 H. Wang, S. Li, Y. Si, N. Zhang, Z. Sun, H. Wu and Y. Lin, *Nanoscale*, 2014, **6**, 8107–8116.
25 S. Li, L. Zhang, Y. Jiang, S. Zhu, X. Lv, Z. Duan and H. Wang, *Nanoscale*, 2017, **9**, 16005–16011.
26 L. Gao, J. Zhuang, L. Nie, J. Zhang, Y. Zhang, N. Gu, T. Wang, J. Feng, D. Yang, S. Perrett and X. Yan, *Nat. Nanotechnol.*, 2007, **2**, 577–583.
27 M. T. Alula, P. Lemmens, L. Bo, D. Wulferding, J. Yang and H. Spende, *Anal. Chim. Acta*, 2019, **1073**, 62–71.
28 N. Mir, P. Karimi, C. E. Castano, N. Norouzi, J. V. Rojas and R. Mohammadi, *Appl. Surf. Sci.*, 2019, **487**, 876–888.
29 F. F. Peng, Y. Zhang and N. Gu, *Chin. Chem. Lett.*, 2008, **19**, 730–733.
30 B. Liu and J. Liu, *Nanoscale*, 2015, **7**, 13831–13835.
31 X. Huang, C. Xu, J. Ma and F. Chen, *Adv. Powder Technol.*, 2018, **29**, 796–803.
32 S. Tang, Y. Li, A. Zhu, Y. Yao, J. Sun, F. Zheng, Z. Lin and W. Shen, *Chem. Commun.*, 2019, **55**, 8386–8389.
33 H. Wang, S. Li, Y. Si, Z. Sun, S. Li and Y. Lin, *J. Mater. Chem. B*, 2014, **2**, 4442–4448.
34 H. Lee, N. F. Scherer and P. B. Messersmith, *Proc. Natl. Acad. Sci. U. S. A.*, 2006, **103**, 12999–13003.
35 N. Holten-Andersen, M. J. Harrington, H. Birkedal, B. P. Lee, P. B. Messersmith, K. Y. Lee and J. H. Waite, *Proc. Natl. Acad. Sci. U. S. A.*, 2011, **108**, 2651–2655.
36 A. Avdeef, S. R. Sofen, T. L. Bregante and K. N. Raymond, *J. Am. Chem. Soc.*, 1978, **16**(100), 17.
37 S. W. Taylor, G. W. Luther and J. H. Waite, *Inorg. Chem.*, 1994, **33**, 5819–5824.
38 R. Li, S. Li, M. Dong, L. Zhang, Y. Qiao, Y. Jiang, W. Qi and H. Wang, *Chem. Commun.*, 2015, **51**, 16131–16134.
39 W. Tang, C. Chen, W. Sun, P. Wang and D. Wei, *Int. J. Biol. Macromol.*, 2019, **128**, 814–824.
40 N. Li, X. Hao, B. H. Kang, Z. Xu, Y. Shi, N. B. Li and H. Q. Luo, *Biosens. Bioelectron.*, 2016, **77**, 525–529.
41 M. Martín, P. Salazar, S. Campuzano, R. Villalonga, J. M. Pingarrón and J. L. González-Mora, *Anal. Methods*, 2015, **7**, 8801–8808.